Appl Nanosci (2015) 5:837–846
DOI 10.1007/s13204-014-0375-5

ORIGINAL ARTICLE

Structural studies and luminescence properties of CeO_2:Eu^{3+} nanophosphors synthesized by oxalate precursor method

G. Vimal · Kamal P. Mani · P. R. Biju · Cyriac Joseph · N. V. Unnikrishnan · M. A. Ittyachen

Received: 26 September 2014 / Accepted: 20 October 2014 / Published online: 8 November 2014

Abstract A novel synthesis strategy to prepare CeO_2:Eu^{3+} nanophosphors and its luminescence behavior is reported. Different structural characterization techniques such as X-ray diffraction, transmission electron microscope and thermogravimetric analysis reveal that thermal decomposition of oxalate precursor is an effective pathway to produce rare earth oxide nanocrystals. Optical characterizations of the CeO_2:Eu^{3+} were done by UV–Visible absorption, photoluminescence excitation and emission spectra. The presence of structural defects and their role on the band gap and luminescence were discussed on the basis of absorption and emission studies. Luminescence study of the CeO_2:Eu^{3+} ensures that the strong charge transfer band of CeO_2 makes it a suitable host material for efficiently exciting Eu^{3+} ions by subsequent energy transfer. The dependence of luminescence efficiency of the CeO_2:Eu^{3+} with varying concentrations of Eu^{3+} was also studied and discussed. The results show that Eu^{3+}-doped CeO_2 nanophosphor is a potential candidate in ultraviolet-based LEDs.

Keywords Oxalate · Nanophosphor · Charge transfer · Photoluminescence · Structural defects

Introduction

Nanophosphors have gained rapid scientific attention owing to their size and shape-dependent physical properties that find wide variety of technological applications in the field of luminescence devices, optical transmission, medical diagnostics, biological fluorescence labels, etc. (Buissette et al. 2006; Bruchez et al. 1998). The novel and distinctive properties of nanophosphors arise due to their quantum confinement and large surface to volume ratio. The luminescent properties such as surface luminescence, emission lifetime, luminescence quantum efficiency and concentration quenching strongly depend on the particle size of the phosphor in the nanoregime (Sun and Murray 1999; Suryanarayana 1995; Kruis et al. 1998; Hase et al. 1990). Hence, in the field of practical phosphors, extensive research has been focused on the synthesis of nanophosphors with improved and consistent efficiency; consequently, the conventional phosphors were replaced by nanophosphors in many of the fields (He et al. 2003; Jose et al. 2005). Rare earth ion activated nanophosphors gained great attention due to their unique optical, magnetic and electronic properties arise from their 4*f* electronic configuration. Rare earth ions are ideal luminescent activators in a variety of host lattices on account of their host independent, sharp 4*f*–4*f* transitions and their ability to produce strong emissions with distinctive colors due to their intra configurational transitions (Chen et al. 2011; Seo et al. 2009; Jose et al. 2007). But the 4*f*–4*f* absorption transitions are parity forbidden and hence it cannot be efficiently excited by the UV LED chips. To overcome this difficulty energy transfer from host material to the activator is an effective option and it is possible only if there is an optimal spectral overlap between the host material and activator. Hence, the selection of host materials and activators are very important to synthesis high performance nanophosphors.

At present, CeO_2 nanostructures aroused much interest because of their strong absorption ability of UV radiation and the subsequent excitation of the activator ions by

G. Vimal · K. P. Mani · P. R. Biju · C. Joseph (✉) · N. V. Unnikrishnan · M. A. Ittyachen
School of Pure and Applied Physics, Mahatma Gandhi University, Kottayam 686560, India
e-mail: cyriacmgu@gmail.com

energy transfer. In addition, both pure and rare earth-ion doped ceria find potential applications as oxygen ion conductors in solid oxide fuel cells, gate oxides in metal oxide semiconductor devices and ultraviolet (UV) blocking materials in UV shielding (Yu et al. 2005; Miki et al. 1990; Tsunekawa et al. 2000). Nanostructured CeO_2 has been prepared by various methods (Sathyamurthy et al. 2005; Yin et al. 2002; Taniguchi et al. 2008; Godinho et al. 2007). However, synthesis of well-dispersed uniform nanocrystals of CeO_2 remains a challenge due to the possibility of agglomeration as well as the high crystalline temperature of the rare earth oxide. Also Eu-doped ceria nanophosphors attracts particular attention as a red emitting phosphor for the application of white light emitting diodes (Fujihara and Oikawa 2004).

Here we introduce a cost effective and simple way to produce Eu^{3+}-doped ceria nanophosphors with uniform size distribution by oxalate decomposition method. The optimal spectral overlap between charge transfer band of the CeO_2 host and the 4*f*–4*f* intraconfigurational transitions of Eu^{3+} encourages effective energy transfer from host to Eu^{3+} ion. Detailed investigations on the luminescent properties such as charge transfer, energy transfer and luminescent quenching occurred on the nanostructured Eu^{3+}-doped ceria were carried out.

Materials and methods

Synthesis

The materials used for the synthesis were cerium nitrate hexahydrate [$(CeNO_3)_3{\cdot}6H_2O$, AR grade, 99.9 %, Alfa Aeser], oxalic acid dehydrate ($H_2C_2O_4{\cdot}2H_2O$, 99 %, Merck) and ethylene glycol (99 %, Merck). Cerium oxide nanocrystals were prepared by thermal decomposition of its oxalate precursor synthesized by microwave-assisted co-precipitation method. Two separate aqueous solutions 25 ml of 0.1 M cerium nitrate and 0.15 M oxalic acid were prepared. Equal amount of ethylene glycol was added to the above solutions and the two solutions were mixed together under vigorous stirring. The whole system was transferred to a microwave oven (2.45 GHz, 700 W), immediately after the formation of a white colloidal solution indicating the nucleation of cerium oxalate crystals. The colloidal solution was subjected to periodic microwave irradiation for 20 s with a time interval of 10 s to enhance the rate of nucleation and encouraging the growth of nanocrystals. After 10 cycles of irradiation, the precipitated solution was taken from the oven and the precipitate was collected by filtration. Cerium oxalate particles thus obtained were washed many times by double distilled water and acetone and then dried at 60 °C for 24 h. The proposed chemical reaction is

$$2Ce(NO_3)_3 + 3H_2C_2O_4 \rightarrow Ce_2(C_2O_4)_3{\cdot}nH_2O + 6HNO_3$$

Controlled thermal decomposition of cerium oxalate precursor was employed to obtain cerium oxide nanocrystals. The calcination temperature was determined based on the results of thermogravimetric analysis of the cerium oxalate. For the preparation of cerium oxide nanocrystals, the synthesized cerium oxalate was calcined at 600 °C for 6 h. During the calcination each building block of the cerium oxalate were decomposed and crystallized as nanocrystals of cerium oxide.

For the preparation of CeO_2:Eu^{3+} (Eu % = 0.5, 1, 1.5, 2), stoichiometric amounts of europium nitrate were added to the aqueous solution of 25 ml of cerium nitrate. The solution was mixed together with ethylene glycol to obtain a homogenous system. Aqueous solution of 25 ml of oxalic acid was prepared and mixed with ethylene glycol. The two solutions were mixed together under vigorous stirring. CeO_2:Eu^{3+} nanocrystals were successfully developed after following the synthesis procedure as described for CeO_2 nanocrystals.

Characterization

The crystallinity of the as prepared samples were determined by X-ray powder diffraction using PANalytical X'Pert Pro diffractometer with Cu Kα radiation ($\lambda = 1.54$ Å). Thermal analysis was done by Perkin Elmer Diamond TG/DTA in the temperature range 50–750 in nitrogen atmosphere. The size of the particles was analyzed using high-resolution transmission electron microscope JEOL JEM 2100. FTIR spectra were recorded using Perkin Elmer Spectrum 400 Spectrometer over the range of 400–4,000 cm^{-1}. UV–Visible diffuse absorption/reflection spectra of the samples were taken by using Perkin Elmer Lambda 650 with 60 mm integrating sphere over the wavelength span of 200–800 nm. The photoluminescence spectra of the synthesized phosphors were taken using Horiba Jobin-Yvon fluoromax4 spectrofluorometer in the wavelength range 360–650 nm.

Results and discussion

Structural studies

X-ray diffraction analysis

The X-ray diffractogram of the pure and doped cerium oxalate given in Fig. 1a are in close agreement with the standard data of Ce_2 $(C_2O_4)_3{\cdot}10H_2O$ (ICDD 200268). Hence, we can assume that the synthesized precursors were

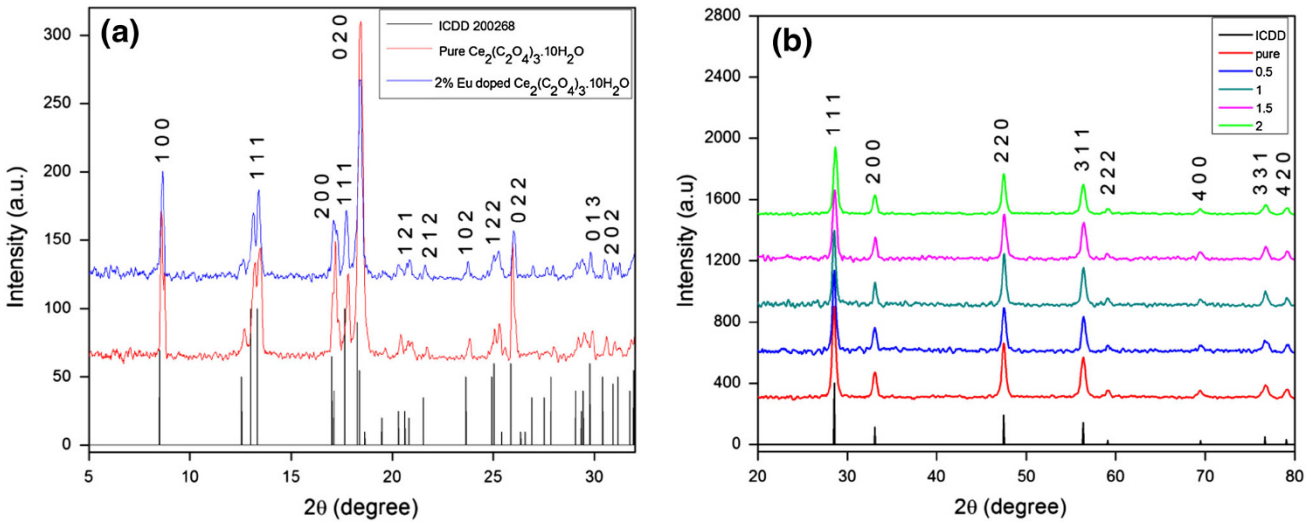

Fig. 1 X-ray diffractograms of the **a** cerium oxalate and 2 % Eu doped cerium oxalate and **b** CeO_2:Eu^{3+} (Eu % = 0.5, 1, 1.5, 2) nanocrystal

crystallized to cerium oxalate decahydrate and the doping of Eu^{3+} does not affect the crystal structure. The X ray diffractogram of the pure CeO_2 and CeO_2:Eu^{3+} (Eu % = 0.5, 1, 1.5, 2) were depicted in Fig. 1b along with their standard data. From the figure, it is observed that doped and pure samples were crystallized in the same structure and is consistent with the standard crystallographic data of face-centered cubic structure of CeO_2 (ICDD 65-2975) with space group $Fm\bar{3}m$. The analysis also reveals the absence of Eu_2O_3 phase in the CeO_2 structure which indicates that Eu^{3+} ions were successfully substituted the Ce^{4+} ions without changing the crystal structure of cubic CeO_2. However, intensity of the diffraction peaks of CeO_2 slightly decreases with the addition of Eu^{3+} ions due to the lattice strain imposed by the dopant.

The crystalline sizes of the products were calculated using the Scherrer equation

$$L = \frac{k\lambda}{\beta \cos\theta} \quad (1)$$

where L is the crystalline size of the material, k is the shape factor, λ is the wavelength used for the analysis, β is the full width at half maximum of the diffraction peak measured in radian and θ is the angle corresponds to the peak. The average crystalline size of pure and doped cerium oxalate were calculated to be 33 and 30 nm, respectively. The average size of the nanocrystals was decreased to 16 nm in the case of pure and CeO_2:Eu^{3+}.

Thermal analysis

Thermal analysis (TG/DTA) of cerium oxalate decahydrate was performed in nitrogen atmosphere to evaluate the thermal decomposition behavior of the precursor and the thermogram was shown in Fig. 2. The decomposition involves three stages ending with the formation of cerium oxide as the stable phase. The first two stages are due to the dehydration of water molecules present in cerium oxalate decahydrate in consistent with the earlier reports on the thermal decomposition of rare earth oxalates (Joseph et al. 1998; Vimal et al. 2014). Between 60 to 140 °C seven water molecules, which are loosely bounded in the crystal lattice, were evaporated and the corresponding mass loss is estimated to be 18.45 %. The three coordinated water molecules were eliminated from the crystal resulting to a mass loss of 7.6 % on raising the temperature up to 300 °C. The experimental mass losses are in good agreement with the calculated mass losses of 17.4 and 7.5 %, which confirms the two stage dehydration process. The third decomposition occurred more rapidly, which is indicated by the sharp exothermic peak in the DTA and is completed around 360 °C with the formation of stable cerium oxide. Slight difference observed between the calculated mass loss of 29 % and experimental loss of 34 % may be due to the evaporation of residuals from ethylene glycol used in the synthesis. After 360 °C, no weight loss was occurred which indicates the stability of the product. The expected thermal decomposition steps of cerium oxalate can be expressed as follows

$$Ce_2(C_2O_4)_3{\cdot}10H_2O \rightarrow Ce_2(C_2O_4)_3 3H_2O + 7H_2O$$
$$Ce_2(C_2O_4)_3 3H_2O \rightarrow Ce_2(C_2O_4)_3 + 3H_2O$$
$$Ce_2(C_2O_4)_3 \rightarrow 2CeO_2 + 2CO_2 + 4CO$$

The presences of seven randomly distributed water molecules and the three coordinated water molecules are well-evidenced by the two-step dehydration processes. Hence, the chemical formula and the hydration number of

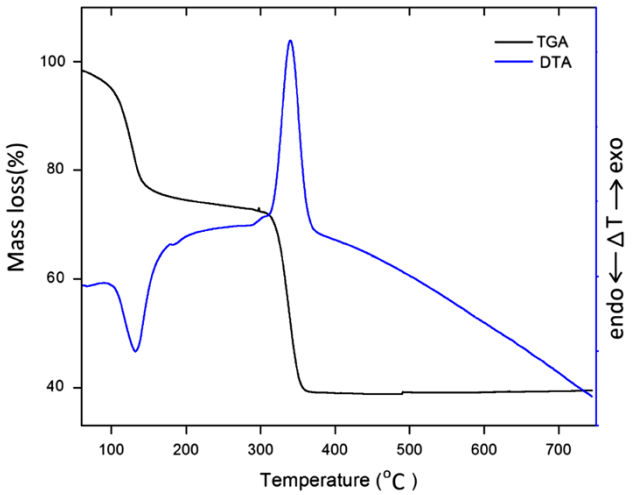

Fig. 2 TG/DTA diagram of the cerium oxalate precursor

the precursor proposed by the X-ray diffraction studies are confirmed by the thermal analysis.

Transmission electron microscopy (TEM)

The size and structure of the crystals were further analyzed by transmission electron microscope (TEM) and the images of pure CeO_2 and CeO_2:Eu (Eu = 2 %) nanocrystals were shown in Fig. 3a and b, respectively. It is observed that uniform sized nanocrystals with spherical morphology and less agglomeration were formed after the thermal decomposition of the oxalate precursor. Histograms representing the size distribution of particle were given as inset. The average size of both CeO_2 and Eu^{3+}-doped CeO_2 nanocrystals were found to be 8–12 nm. The images and the histogram of the nanocrystals suggest that doping of Europium ions does not influence the size or morphology of the crystal. The high-resolution TEM image given in Fig. 3c displays the lattice fringes of CeO_2 nanocrystals, which confirms the high crystallinity of the nanocrystals. The selected area electron diffraction (SAED) pattern (inset of 3c) shows the (200), (220) and (311) planes of the nanocrystal which are in good agreement with the XRD result of cubic CeO_2. Image of typical spherical nanocrystal of cerium oxide was given in Fig. 3d. Hence from the TEM analysis, we can confirm that thermal decomposition of oxalate precursor is an effective and reliable method to synthesis homogeneous rare earth oxide nanocrystals.

Based on the thermogravimetric and transmission electron microscopic analysis it is confirmed that homogenous spherical nanocrystals of pure and doped ceria with less agglomeration can be obtained by the thermal decomposition of their respective oxalates. The thermal decomposition of oxalate precursor is a widely accepted method for the synthesis of nanocrystals of transition metal oxides (Niasari et al. 2009; Ren et al. 2009). In our previous work (Vimal 2014), we have reported the formation of nanostructured samarium oxalate. In this work also microwave-assisted co precipitation method was employed to prepare nanocrystals cerium oxalate which are aggregated together oriently to form the nanostructured cerium oxalate. The as formed nanostructures when subjected to annealing at 450 °C, the aggregation becomes fragmented, along with the decomposition of oxalate by the elimination of H_2O, CO_2 and CO leading to the formation of oxide nanocrystals. Scheme 1 illustrates the possible formation mechanism of cerium oxide nanocrystals from the precursor.

Fourier transform infrared spectroscopy (FTIR)

Figure 4a shows the Fourier transform infrared spectrum of the $Ce_2(C_2O_4)_3{\cdot}10H_2O$ precursor. The spectrum exhibits a broad band in the region 3,000–3,600 cm^{-1} due to the presence of water molecules (ν(O–H)). The very strong peak observed at 1,620 cm^{-1} is attributed to the combined effect of asymmetric stretching vibrations of C=O and the bending of water molecules. The strong peak observed at 1,320 cm^{-1} is due to the asymmetric stretching of CO_2 molecule associated with the oxalate ligand. The metal oxygen bond is evidenced by the absorption at the wavenumber 800 and 500 cm^{-1} (Elizabeth et al. 2005; Petrov and Soptrajanov 1975; Fujita et al. 1962). The FTIR spectra of the pure CeO_2 and that doped with different concentrations of Eu^{3+} were given in Fig. 3b. It is observed that the spectra of the CeO_2:Eu^{3+} nanocrystals show identical spectral behavior of that of pure ceria regardless of their doping concentration. In the case of cerium oxide, most of the peaks of carbonate groups are disappeared after the decomposition of oxalate. Very feeble peaks observed between 1,200 and 1,700 cm^{-1} are due to the residual carbonate groups present in the cerium oxide. The broad and weak band around 3,300 cm^{-1} is attributed to the physiosorbed water molecules present in the material. (Mokkelbost et al. 2004).

Optical study

UV–Visible absorption

The UV–Visible absorption spectra of the CeO_2:Eu^{3+} (Eu % = 0.5, 1, 1.5, 2) were shown in Fig. 5 which reveal the strong ultra violet absorption ability of cerium oxide attributed to the charge transfer from O^{2-} to Ce^{4+} ions.

The absorption edge of the Eu^{3+}-doped CeO_2 does not show any shift from that of the pure ceria. The band gap of the pure and doped cerium oxide nanocrystals were determined from the equation

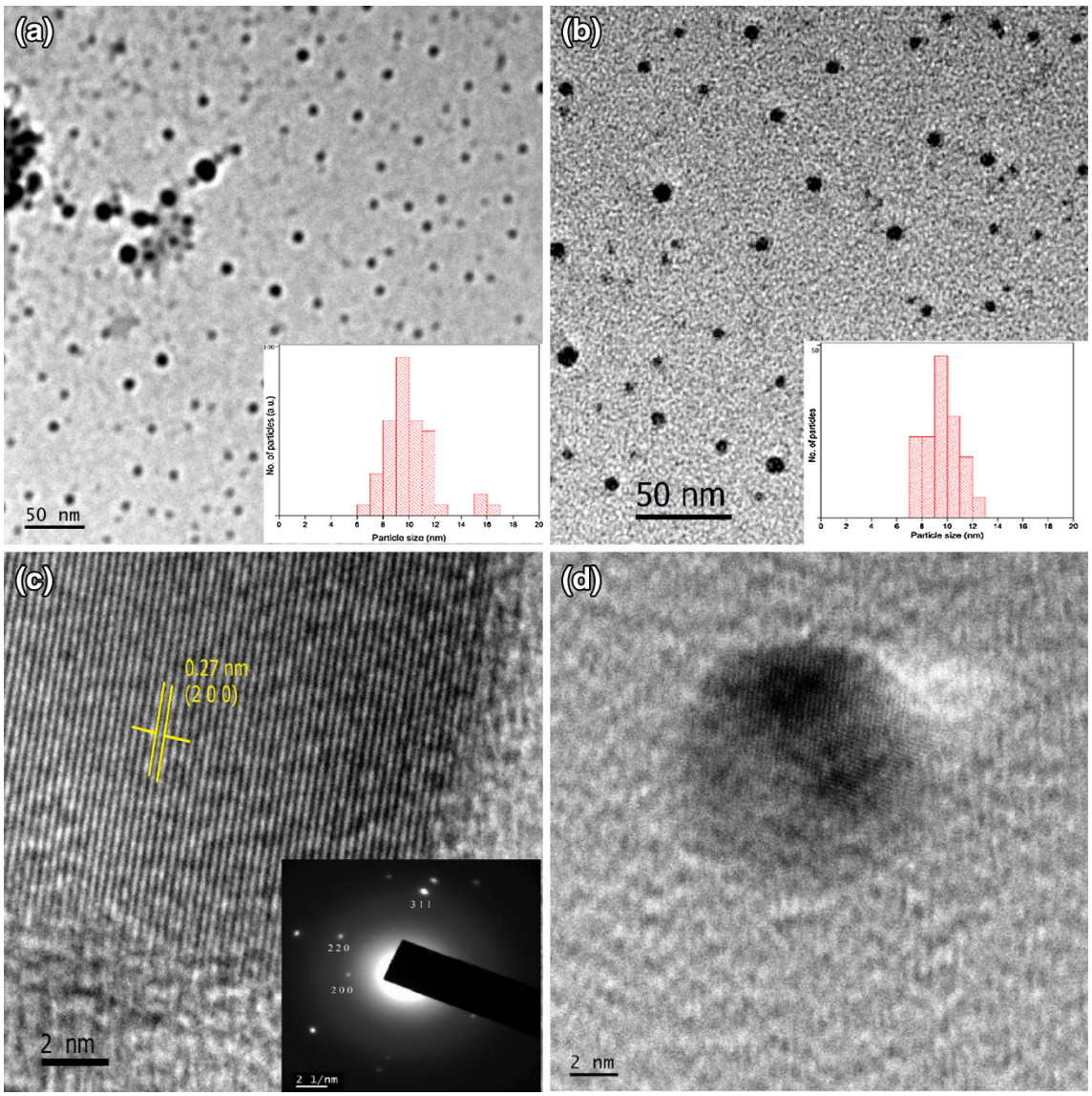

Fig. 3 Transmission electron microscope image of the nanocrystals. **a** CeO_2 nanocrystals and particle size histogram (*inset*), **b** CeO_2:Eu (Eu % = 2) nanocrystals and particle size histogram (*inset*), **c** HRTEM and SAED (*inset*) of the CeO_2 crystal and **d** image of the typical spherical CeO_2 nanocrystal

$$\alpha hv = A\left(hv - E_g\right)^{\frac{1}{2}} \quad (2)$$

where α is the optical absorption coefficient, hv is the photon energy, E_g is the direct band gap, and A is a constant. Band gap of the sample were calculated by plotting $(\alpha hv)^2$ as a function of hv and extrapolating the linear portion of the curve towards x-axis. From the plot, the band gaps of the both pure and doped nanocrystals were estimated to be 2.6 eV that is quite different from that of the bulk ceria (3.2 eV). This behavior is rather interesting as a red shift is observed in the band gap of the cerium oxide nanocrystals in spite of the expected blue shift due to the quantum confinement. The reason for the red shift is strongly correlated with the existence of Ce^{3+} ions in the CeO_2 structure. The Ce^{3+} ions are generated due to the large surface to volume ratio of the nanocrystals, which eases the break out of oxygen and promotes the reduction of Ce^{4+} to Ce^{3+}. Hence small amount of Ce^{3+} ions are coexisted with the Ce^{4+} in the structure and Ce^{3+}/Ce^{4+} ratio increases with the decrease of particle size of the nanocrystal (Wu et al. 2004; Patsalas and Logothetidis 2003; Ansari et al. 2014). Introduction of Ce^{3+} leads to the oxygen ion vacancy and defects on the external surface of the particle, which influences the band gap. Hence, the expected blue shift due to the quantum confinement effect may overcome by the red shift induced by the Ce^{3+} ions and defects.

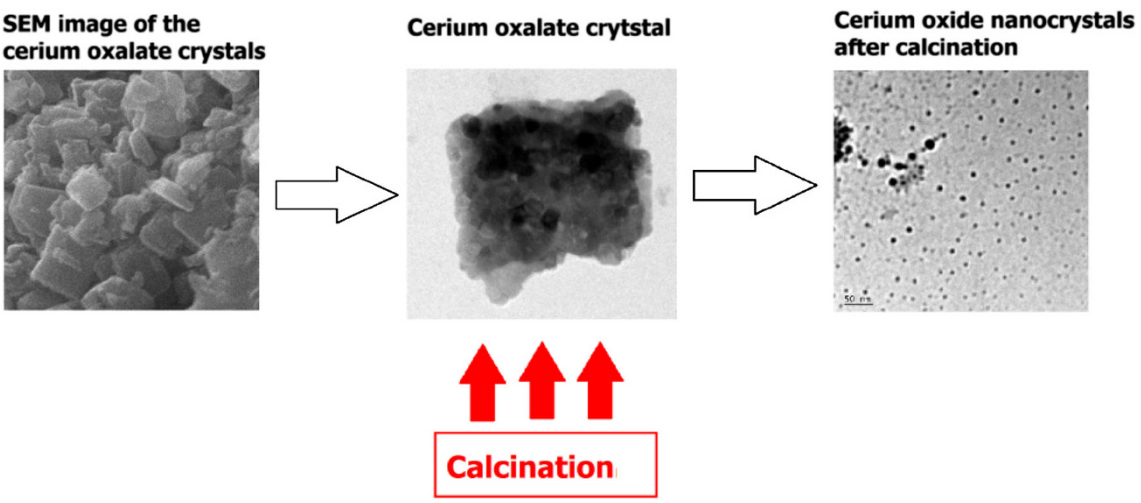

Scheme 1 Schematic representation of the formation of cerium oxide nanocrystals from cerium oxalate crystals

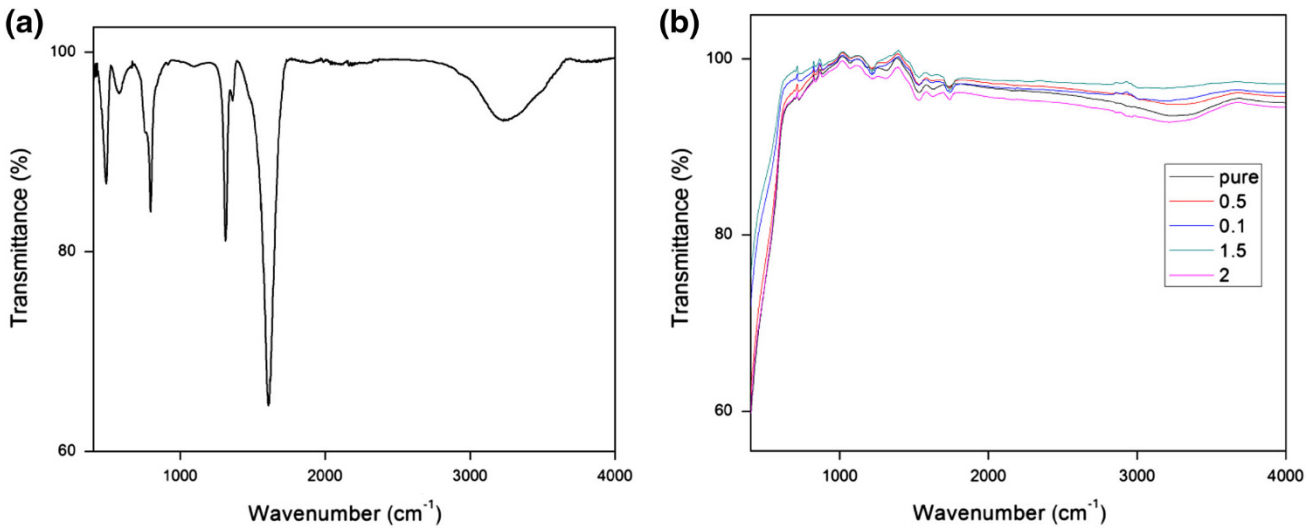

Fig. 4 FTIR spectra of the **a** cerium oxalate precursor and **b** CeO_2:Eu^{3+} (Eu % = 0.5, 1, 1.5, 2) nanocrystal

Luminescence spectra

The excitation and emission spectra of the $Ce_2(C_2O_4)_3{\cdot}10\ H_2O$:Eu with different doping concentration of 0.5, 1, 1.5 and 2 % were shown in Fig. 6. The excitation spectra were taken by fixing the emission at 617 nm and the spectra exhibits two dominant peaks at 393 and 463 nm corresponds to f–f transition of Eu^{3+} ion $^7F_0 \rightarrow {}^5L_6$ and $^7F_0 \rightarrow {}^5D_2$, respectively. Emission spectra were obtained by exciting the material with a wavelength of 393 nm. Three emission peaks observed at 592, 617 and 649 nm are due to the transitions from $^5D_0$ to $^7F_1$, $^7F_2$ and $^7F_3$ levels respectively. From the figure, it can be seen that the emission is maximum at the wavelength 617 nm and the optimum doping concentration is 1.5 % europium. For the dopant concentration of 2 %, an emission quenching is observed.

In view of their potential use as optical materials, the luminescence properties of CeO_2 and CeO_2:Eu^{3+} nanophosphors were investigated by photoluminescence spectra. To obtain the emission spectra, pure CeO_2 were excited by the radiation of wavelength 337 nm and the spectrum exhibits broad emission in the region 350–500 nm as shown in Fig. 7. It is evident that the emission is not promoted by f-d transition or charge transfer of Ce^{4+} because the emission of Ce^{4+} usually lies in the region 490–550 nm. Also the spectrum can be fitted as the resultant of two sub peaks with a wavelength 419 and 462 nm by deconvolution process using Gaussian. The energy separation between the two sub peaks (2,200 cm^{-1})

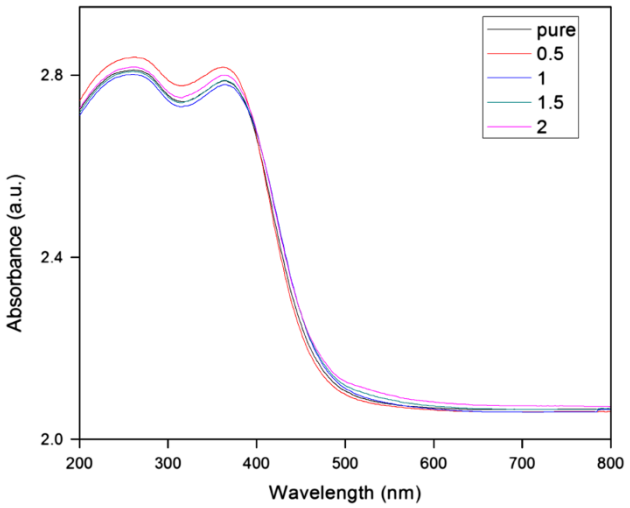

Fig. 5 UV–Visible absorption spectra of the CeO_2:Eu^{3+} (Eu % = 0.5, 1, 1.5, 2) nanocrystals

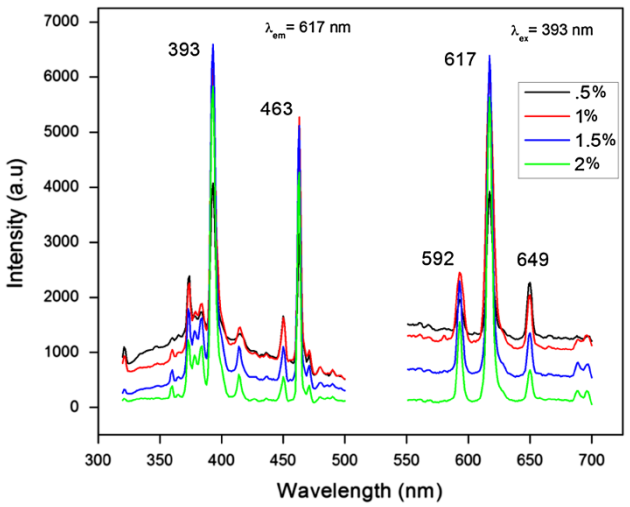

Fig. 6 Photoluminescence excitation and emission spectra of the $Ce_2(C_2O_4)_3{\cdot}10H_2O$: Eu^{3+} (Eu % = 0.5, 1, 1.5, 2)

is comparable to the energy difference between the $^2F_{5/2}$ and $^2F_{7/2}$ sublevels of the ground state of Ce^{3+} ion in crystals (2,000 cm^{-1}) (Xie et al. 2004; Bahadur et al. 2013). Hence, we can assume that the peaks arise due to the transition from the lower levels of $5D^1$ states to $^2F_{5/2}$ and $^2F_{7/2}$ sublevels of the ground state of Ce^{3+} ions. In addition, the defects like oxygen ion vacancies in the crystal also contribute to the emission in the spectral region 350–500 nm (Phokha et al. 2012).

Excitation and emission spectra of the CeO_2:Eu^{3+} for different dopant concentrations (Eu % = 0.5, 1, 1.5, 2) were shown in Figs. 8 and 9. The excitation spectra were obtained by monitoring the prominent emission of Eu^{3+} at the wavelength 592 nm. The spectra exhibit a wide and strong excitation band in the wavelength region

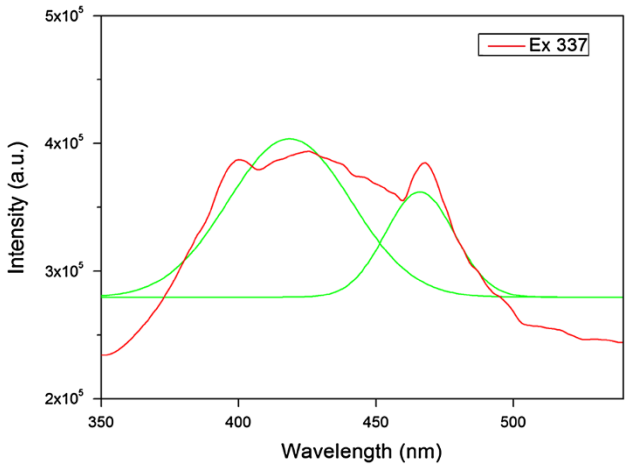

Fig. 7 Photoluminescence spectra of the CeO_2

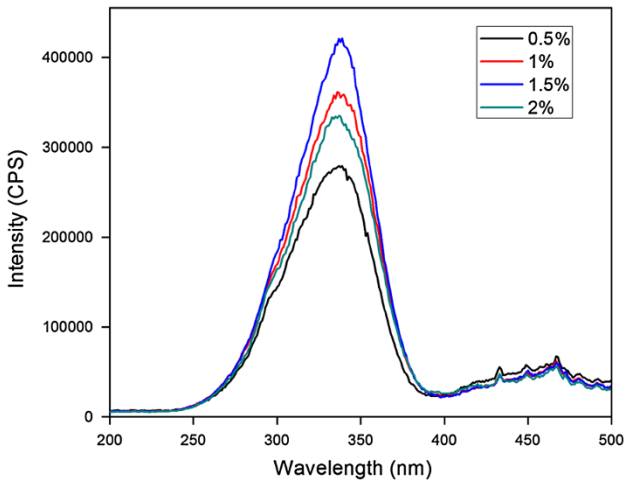

Fig. 8 Photoluminescence excitation spectra of the CeO_2:Eu^{3+} (Eu % = 0.5, 1, 1.5, 2)

300–370 nm and are ascribed to the charge transfer from O^{2-} to Ce^{4+}. Excitation peaks due to the *f–f* transitions of Eu^{3+} are observed in the range 390–480 nm (Qing et al. 2011).Very weak *f–f* transitions of Eu^{3+} revealed that the excitation of Eu^{3+} ions was occurred purely by the energy transfer from Ce^{4+}. Hence we can suggest that the CeO_2 host material can acquire energy from the *n*-UV excitation and able to transfer energy to Eu^{3+} ions ensuing the red emission of CeO_2:Eu^{3+} nanophosphors. The optimal spectral overlap of CeO_2 and Eu^{3+} is very important to get the efficient energy transfer. Strong and intense red light in the emission spectra reveals that the energy levels of Eu^{3+} are suitable to accept energy from Ce^{4+} which can be excited by charge transfer upon exciting with UV light.

The emission spectra of the Eu-doped CeO_2 nanophosphors exhibit broad emission in the region 350–500 nm due to the presence of Ce^{3+} and defects as discussed earlier and the sharp emissions at higher wavelengths are due to the

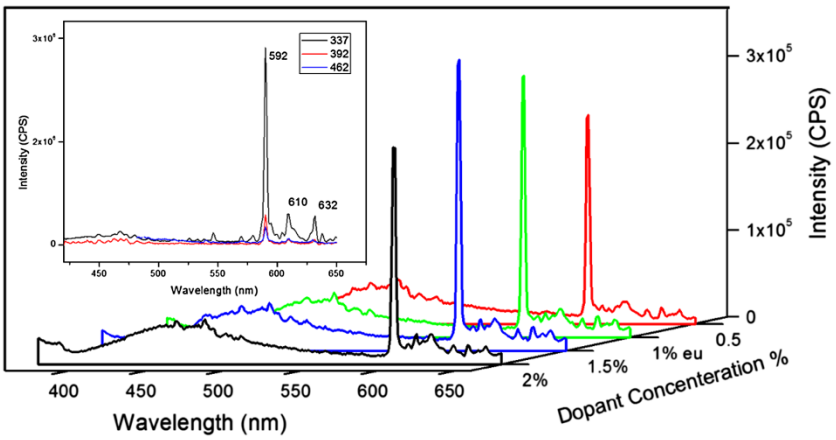

Fig. 9 Photoluminescence emission spectra of the CeO_2:Eu^{3+} (Eu % = 0.5, 1, 1.5, 2)

f–f transitions of Eu^{3+} ions. The emission peaks present in the spectra at 592, 610 and 632 nm can be assigned due to the intraconfigurational *f–f* transition of Eu^{3+} from $^5D_0$ to different ^7F_J levels (where $J = 1, 2$ and 3) and the emission at 592 nm shows the maximum intensity (35). The strong characteristic peak of Eu^{3+} due to $^5D_0 \rightarrow {}^7F_2$ transition is very weak in the Eu-doped cerium oxide nanocrystals. This is due to the inversion symmetry of the site occupied by Ce^{4+}. In CeO_2 fluorite structure, the site occupied by Ce^{4+} has ideally Oh symmetry with eightfold oxygen coordination. When Ce^{4+} ions were substituted by Eu^{3+} ions, its transitions are influenced by the inversion symmetry of the site. According to the Judd–Ofelt theory, the electric dipole transitions are only allowed in the absence of inversion symmetry. Therefore, the electric dipole transition would be forbidden and could not observe in the spectra (Judd 1962; Ofelt 1962). Magnetic dipole transitions are not affected by the site symmetry of the surrounding lattice and hence the magnetic dipole transition $^5D_0 \rightarrow {}^7F_1$ at 592 nm dominates. However, doping creates symmetry distortions in the environment around Eu^{3+} and this partially allows the electric dipole transitions. Thus, the electric dipole transitions $^5D_0 \rightarrow {}^7F_2$ and $^5D_0 \rightarrow {}^7F_3$ of Eu^{3+} are observed in the spectra at 610 and 632 nm with very low intensity.

The intensity of the dominant peak 592 nm attains its maximum at the doping concentration of 1.5 %. Further increasing of the concentration of Eu^{3+} diminishes the emission intensity. The excitation spectrum also shows the same behavior. This is due to the high concentration of europium ions, which leads to concentration quenching and reduction in luminescence efficiency. On increasing concentration, the distance between the Eu^{3+} ions become shorter and energy migrates to a longer extent. Presence of defect sites in the path of the energy migration promotes the non-radiative relaxation and this will lead to the decrease of luminous intensity. The inset of the Fig. 9 shows a comparison between the emission spectrum obtained by exciting the charge transfer band and the *f–f* transition of Eu^{3+} (392 and 463 nm) for CeO_2:Eu^{3+} (Eu % = 1.5). From the figure it is obvious that the emission of Eu^{3+} by exciting the charge transfer band is highly intense than the emission by direct excitation. In addition, the spectrum implies that the charge transfer process is the only effective pathway to efficiently excite the Eu^{3+} ions and the suitability of the CeO_2 as a host material.

The emission spectra of the CeO_2:Eu^{3+} nanophosphor is completely different from that of the Eu-doped cerium oxalate precursor. The difference arises due to the inversion symmetry of the site possessed by the Eu^{3+} ion in the CeO_2 lattice. Due to the lack of inversion symmetry both the magnetic dipole and electric dipole transitions, were observed in the emission spectra of the Eu^{3+}-doped cerium oxalate. The electric dipole transition $^5D_0$–$^7F_2$ appeared at 617 nm possess the maximum intensity upon an excitation at 393 nm. In the case of CeO_2:Eu^{3+}, the whole spectrum changes due to the presence of the inversion symmetry. The electric dipole transitions became faint and the magnetic dipole transition possessed the maximum intensity. Most importantly intense and wide charge transfer band was availed to excite the Eu^{3+} instead of exciting the narrow *f–f* band. Due to the strong ultraviolet absorption ability of the CeO_2 and due to the optimal spectral overlap between the charge transfer band of CeO_2 and *f–f* transitions of Eu^{3+}, the intensity of the emission at 592 nm is greatly enhanced. Thus, the charge transfer band opens the possibility of the wide excitation range, which is very important in the field of optical applications.

Conclusions

Nanophosphors of CeO_2:Eu^{3+} with different dopant concentrations were successfully synthesized by thermal decomposition of oxalate precursor. X-ray diffractograms reveal that all the CeO_2:Eu^{3+} nanophosphors were crystallized in the cubic phases of CeO_2. The well-dispersed

nanocrystalline behavior of the particles is confirmed by the transmission electron microscope imaging. The thermal and microscopic analysis suggests that the method is very effective and suitable for the synthesis of rare earth oxide nanocrystals. The functional groups were identified by the Fourier transform infrared spectra of the nanocrystal. Surface defects on the nanocrystal hold an important role in the optical properties. Due to the presence of defects like oxygen ion vacancies, the band gap of the cerium oxide nanocrystal is red shifted to 2.6 eV compared to that of the bulk ceria. The defects and the presence of Ce^{3+} ions promote broad emission in the region from 350 to 500 nm. A comparison between the emission spectra of precursor and the CeO_2:Eu^{3+} was done. The results infer that, in CeO_2:Eu^{3+} nanocrystals, the strong charge transfer band overcomes the limitation of narrow *f–f* absorption efficiency and Eu^{3+} ions can be effectively excited by *n*-UV LEDs. Due to the inversion symmetry of the site possessed by Eu^{3+} ions in the CeO_2 structure the magnetic dipole transition is dominated in the fluorescence spectra. Maximum emission intensity is observed for the dopant concentration of 1.5 % and after that, emission is quenched. Hence based on the optical properties, the CeO_2:Eu^{3+} nanocrystals can be considered as a potential phosphor material for optical applications.

Acknowledgments The authors are thankful to UGC (Govt. of India) and DST (Govt. of India) for the financial assistance through SAP-DRS and DST-PURSE programs, respectively. The authors Vimal G and Kamal P Mani are thankful to University Grants Commission, Govt. of India for the award of RFSMS fellowship. The authors are also thankful to SAIF KOCHI for TG/DTA analysis.

References

Ansari SA, Khan MM, Ansari MO, Kalathil S, Lee J, Cho MH (2014) Band gap engineering of CeO_2 nanostructure using an electrochemically active biofilm for visible light applications. Res Adv 4:16782–16791. doi:10.1039/c4ra00861h

Bahadur A, Dwivedi Y, Rai SB (2013) Optical properties of cerium doped oxyfluoroborate glass. Spectrochim Acta A 110:400–403. doi:10.1016/j.saa.2013.03.066

Bruchez MP, Moronne M, Gin P, Weiss S, Alivisatos AP (1998) Semiconductor nanocrystals as fluorescent biological labels. Science 281:2013–2016. doi:10.1126/science.281.5385.2013

Buissette V, Giaume D, Gacoin T, Boilot JP (2006) Aqueous routes to lanthanide-doped oxide nanophosphors. J Mater Chem 16:529–539. doi:10.1039/b508656f

Chen Y, Wang J, Liu C, Kuang X, Su Q (2011) A host sensitized reddish-orange Gd $_2$ MoO_6:Sm^{3+} phosphor for light emitting diodes. Appl Phys Lett 98:081917

Elizabeth A, Joseph C, Paul I, Ittyachen MA, Mathew KT, Lonappan A, Jacob J (2005) Microwave studies on double rare earth oxalate crystals. Mater Sci Eng A 391:43–50

Fujihara S, Oikawa M (2004) Structure and luminescent properties of CeO2: rare earth (RE = Eu3+ and Sm3+) thin films. J Appl Phys 95:8002–8006. doi:10.1063/1.1751240

Fujita J, Martell AE, Nakamoto K (1962) Infrared spectra of metal chelate compounds. VII. Normal coordinate treatments on 1:2 and 1:3 oxalato complexes. J Chem Phys 36: 331–338. doi:10.1063/1.1732505

Godinho MJ, Gonçalves RF, Santos LPS, Varela JA, Longo E, Leite ER (2007) Room temperature co-precipitation of nanocrystalline CeO_2 and $Ce_{0.8}Gd_{0.2}O_{1.9-\delta}$ powder. Mater Lett 61:1904–1907. doi:10.1016/j.matlet.2006.07.152

Hase T, Kano T, Nakazawa E, Yamamoto H (1990) Phosphor materials for cathode-ray tubes. Adv Electr Phys 79:271–373. doi:10.1016/S0065-2539(08)60600-9

He C, Guan Y, Yao L, Cai W, Li X, Yao Z (2003) Synthesis and photoluminescence of nano-Y_2O_3:Eu^{3+} phosphors. Mater Res Bull 38:973–979

Jose G, Thomas V, Fernandez TT, Adiyodi AK, Joseph C, Ittyachen MA, Unnikrishnan NV (2005) Radiative parameters of Eu^{3+}ions in CdSe nanocrystal containing silica matrices. Phys B 357:270–276. doi:10.1016/j.physb.2004.11.075

Jose G, Joseph C, Ittyachen MA, Unnikrishnan NV (2007) structural and optical characterization of CdSe nanocrystallites/rare earth ions in sol–gel glasses. Opt Mater 29:1495–1500

Joseph C, Varghese G, Ittyachen MA (1998) J Thermal Anal 52:517–522

Judd BR (1962) Optical absorption intensities of rare-earth ions. Phys Rev 127:750–761. doi:10.1103/PhysRev.127.750

Kruis FE, Fissan H, Peled AJ (1998) Synthesis of nanoparticles in the gas phase for electronic, optical and magnetic applications—a review. Aerosol Sci 29:511–535. doi:10.1016/S0021-8502(97)10032-5

Miki T, Ogawa T, Haneda M, Kakuta N, Ueno A, Tateishi S, Matsuura S, Sato M (1990) Enhanced oxygen storage capacity of cerium oxides in CeO_2/La_2O_3/AI_2O, containing precious metals. J Phys Chem 94:6464–6467. doi:10.1021/j100379a056

Mokkelbost T, Kaus I, Grande T, Einarsrud MA (2004) Combustion synthesis and characterization of nanocrystalline CeO_2-based powders. Chem Mater 16:5489–5494. doi:10.1021/cm048583p

Niasari MS, Mohandes F, Davar F (2009) Preparation of PbO nanocrystals via decomposition of lead oxalate. Polyhedron 28:2263–2267. doi:10.1016/j.poly.2009.04.009

Ofelt GS (1962) Intensities of crystal spectra of rare-earth ions. J Chem Phys 37:511. doi:10.1063/1.1701366

Patsalas P, Logothetidis S (2003) Structure-dependent electronic properties of nanocrystalline cerium oxide films. Phys Rev B 68: 035104 (1–13). doi: 10.1103/PhysRevB.68.035104

Petrov I, Soptrajanov B (1975) Infrared spectrum of whewellite. Spectrochim Acta A 31:309–316. doi:10.1016/0584-8539(75)80025-0

Phokha S, Pinitsoontorn S, Chirawatkul P, Pooarporn Y, Maensiri S (2012) Synthesis, characterization, and magnetic properties of monodisperse CeO_2 nanospheres prepared by PVP-assisted hydrothermal method. Nanoscale Res Lett 7:425 (1–13). doi:10.1186/1556-276X-7-425

Qing Z, Qingyu M, Yue T, Xiaohui F, Jiangting S, Shuchen L (2011) Luminescent properties of Eu^{3+} doped Gd_2WO_6 and $Gd_2(WO_4)_3$ nanophosphors prepared via co-precipitation method. J Rare Earths 29:815–821. doi:10.1016/S1002-0721(10)60566-2

Ren L, Wang P, Han Y, Hua C, Wei B (2009) Synthesis of $CoC_2O_42H_2O$ nanorods and their thermal decomposition to Co_3O_4 nanoparticles. Chem Phys Lett 476: 78–83. doi:10.1016/j.cplett.2009.06.015

Sathyamurthy S, Leonard KJ, Dabestani RT, Paranthaman MP (2005) Reverse micellar synthesis of cerium oxide nanoparticles.

Nanotechnology 16:1960–1964. doi:10.1088/0957-4484/16/9/089

Seo S, Yang H, Holloway PH (2009) Controlled shape growth of Eu- or Tb-doped luminescent Gd_2O_3 colloidal nanocrystals. J Colloid Interface Sci 331:236–242. doi:10.1016/j.jcis.2008.11.016

Sun S, Murray CB (1999) Synthesis of monodisperse cobalt nanocrystals and their assembly into magnetic super lattices (invited). J Appl Phys 85:4325–4330. doi:10.1063/1.37035

Suryanarayana C (1995) Nanocrystalline materials. Int Mater Rev 40:41–64

Taniguchi T, Watanabe T, Sakamoto N, Matsushita N, Yoshimura M (2008) Aqueous route to size-controlled and doped organophilic ceria nanocrystals. Cryst Growth Des 8:3725–3730. doi:10.1021/cg800363w

Tsunekawa S, Fukuda T, Kasuya A (2000) Blue shift in ultraviolet absorption spectra of monodisperse CeO_{2-x} nanoparticles. J Appl Phys 87:1318–1321. doi:10.1063/1.372016

Vimal G, Kamal PM, Biju PR, Joseph C, Unnikrishnan NV, Ittyachen MA (2014) Synthesis, structural and spectroscopic investigations of nanostructured samarium oxalate crystals. Spectrochim Acta A 122: 624–630. doi:10.1016/j.saa.2013.11.080

Vimal G, Kamal PM, Jose G, Biju PR, Joseph C, Unnikrishnan NV, Ittyachen MA (2014b) Growth and spectroscopic properties of samarium oxalate single crystals. J Cryst Growth 404:20–25. doi:10.1016/j.jcrysgro.2014.06.041

Wu LJ, Wiesmann HJ, Moodenbaugh AR, Klie RF, Zhu Y, Welch DO, Suenaga M (2004) Oxidation state and lattice expansion of CeO_{2-x} nanoparticles as a function of particle size. Phys Rev B 69: 125415 (1–9). doi:10.1103/PhysRevB.69.125415

Xie RJ, Hirosaki N, Mitomo M, Yamamoto Y, Suehiro T, Ohashi N (2004) Photoluminescence of cerium-doped SiAlON materials. J Am Ceram Soc 87:1368–1370

Yin L, Wang Y, Pang G, Koltypin Y, Gedanken A (2002) Sonochemical synthesis of cerium oxide nanoparticles—effect of additives and quantum size effect. J Colloid Interface Sci 246:78–84. doi:10.1006/jcis.2001.8047

Yu T, Joo J, Park YI, Hyeon T (2005) Large-scale nonhydrolytic sol–gel synthesis of uniform-sized ceria nanocrystals with spherical, wire, and tadpole shapes. Angew Chem Int Ed 44:7411–7414. doi:10.1002/anie.200500992